Journal of Molecular Graphics and Modelling 38 (2012) 112–122

Contents lists available at SciVerse ScienceDirect

Journal of Molecular Graphics and Modelling

journal homepage: www.elsevier.com/locate/JMGM

Exploring the structure determinants of pyrazinone derivatives as PDE5 3HC8 inhibitors: An in silico analysis

Yan Li[a,*,1], Wenzhao Wu[a,1], Hong Ren[b,c], Jinghui Wang[a], Shuwei Zhang[a], Guohui Li[c,*], Ling Yang[d]

[a] Department of Materials Science and Chemical Engineering, Dalian University of Technology, Dalian, Liaoning 116023, China
[b] Department of Ophthalmology, Qi Lu Hospital, Medical School of Shandong University, Jinan 250012, China
[c] Laboratory of Molecular Modeling and Design, State Key Laboratory of Molecular Reaction Dynamics, Dalian Institute of Chemical Physics, Chinese Academy of Sciences, Dalian 116023, China
[d] Laboratory of Pharmaceutical Resource Discovery, Dalian Institute of Chemical Physics, Graduate School of the Chinese Academy of Sciences, Dalian, Liaoning 116023, China

ARTICLE INFO

Article history:
Accepted 3 July 2012
Available online 16 July 2012

Keywords:
PDE5
Pyrazinone-based inhibitors
3D-QSAR
Molecular docking
Molecular dynamics

ABSTRACT

Phosphodiesterase type 5 (PDE5) inhibitors are clinically indicated for the treatment of erectile dysfunction, pulmonary hypertension and various other diseases. In this work, both ligand- and receptor-based three-dimensional quantitative structure–activity relationship (3D-QSAR) studies were carried out using comparative molecular field analysis (CoMFA) and comparative molecular similarity indices analysis (CoMSIA) techniques on 122 pyrazinone derivatives as PDE inhibitors. The resultant optimum 3D-QSAR model exhibits a proper predictive ability as indicated by the statistical results of Q^2 of 0.584, R^2_{ncv} of 0.884 and R^2_{pre} of 0.817, respectively. In addition, docking analysis and molecular dynamics (MD) simulation were also applied to elucidate the probable binding modes of these inhibitors. Our main findings are: (1) Introduction of bulky, electropositive and hydrophobic substituents at 12- and 19-positions can increase the biological activities. (2) N atom at 8-position is detrimental to the inhibitor activity, and the effect of N atoms at 5- and 6-positions on compound activity is co-determined by both the hydrophobic force and the π–π stacking interaction. (3) Bulky and hydrophilic substitutions are favored at the 27-position of ring D. (4) Electronegative and hydrophilic substitutions around 5- and 6-positions increase the inhibitory activity. (5) Hydrophobic forces and π–π stacking interaction with Phe786 and Phe820 are crucial in determining the binding of pyrazinone derivatives to PDE5. (6) Bulky substitutions around ring C favors selectivity against PDE11, while bulky groups near the 21-position disfavor the selectivity. The information obtained from this work can be utilized to accurately predict the binding affinity of related analogues and also facilitate future rational designs of novel PDE5 inhibitors with improved activity and selectivity.

1. Introduction

Cyclic guanidine monophosphate (cGMP), a second messenger for nitric oxide and atrial natriuretic peptide, signals molecules that are significant for the regulation of various physiological processes, including smooth muscle tone, visual transduction, platelet aggregation, bone growth, electrolyte and fluid homeostasis [1]. Abnormal low levels of cGMP will fail to effectively activate the cGMP-dependent protein kinases, which accordingly disables the regulation of the above physiological processes [2]. Notably, phosphodiesterase type 5 (PDE5), a hydrolase widely expressed in lung, smooth muscle, platelets and kidney, is responsible for the breakdown of cGMP through the hydrolyzation of cGMP to inactive metabolite 5′-GMP, resulting in the decrease of cGMP level [3,4]. Researches have shown that a variety of diseases such as male erectile dysfunction (MED, the most commonly encountered form of sexual dysfunction in men), pulmonary hypertension, memory retention and diabetes are due to the lowering of cGMP level induced by PDE5 [5–9]. Therefore, development of PDE5 inhibitors was recognized as a possible approach to treat such diseases and is by far still the focus of study [4].

Sildenafil (IC_{50} = 3.5 nM), a known selective and potent inhibitor of PDE5 for the treatment of male erectile dysfunction, was the prototypical member of the PDE5 inhibitors [9,10]. In the wake of sildenafil, tadalafil and vardenafil were designed and added to clinical knowledge; these three medicines represent the first-generation of PDE5 inhibitors, used primarily as remedies for MED, and they also have some medical applications in the treatment of pulmonary hypertension, cardioprotection, memory retention and diabetes [6,7,11–15]. In spite of their commercial success, clinical uses have shown significant side effects such as headache, flushing,

* Corresponding authors. Tel.: +86 411 84986062.
E-mail address: yanli@dlut.edu.cn (Y. Li).
[1] Co-first author.

1093-3263/$ – see front matter © 2012 Elsevier Inc. All rights reserved.
http://dx.doi.org/10.1016/j.jmgm.2012.07.003

non-specific gastrointestinal problems, rhinitis and abnormalities of color vision, most of which are related to the insufficient selectivity versus other PDEs [16–18]. Additionally, many PDE5-related diseases require chronic dosing, thus further highlighting the need for second generation of PDE5 inhibitors with improved selectivity and extended duration of action [19].

Up to date, among the great many researches that have been devoted to the development of the second generation of PDE5 inhibitors, the early ones were mainly carried out based on the structure of sildenafil, the traditional drug candidate. The optimization of the sildenafil pyrazolopyrimidinone template and introduction of chirality together with molecular weight reduction led to the discovery of UK-343664 (IC_{50} = 1.1 nM) and UK-371800 (IC_{50} = 4.2 nM) which displayed improved potency and selectivity, but with oral pharmacokinetics found to be non-linear across the dosing range, with wide variations in key parameters [20,21]. Later studies expanded the horizon to other chemicals such as cyclic guanine and pyridopurinone derivatives [18,22]. Recently, Pfizer Global Research and Development has reported the discovery, design and synthesis of a number of potent pyrazinone-based PDE5 inhibitors including 30 amino substituted pyrido[3,2b]pyrazinones, among which are a handful of compounds with improved potency and selectivity over the closely related isoforms PDE6 and PDE11, compared with sildenafil [23]. On such a basis, further structural modifications to the pyrazinone ring system led to the discovery of 5 new compounds with enhanced physicochemical properties, in particular solubility [24]. Nonetheless, these chemicals suffered from an undesired pharmacokinetic (PK) profile and successive efforts to improve the PK profile culminated in the discovery of 45 novel compounds, of which 3-[(trans-4-hydroxycyclohexyl)amino]-7-(6-methoxypyridin-3-yl) -1-(2-propxyethyl)pyrido[3,4-b]pyrazin-2(1H)-one (**53**, IC_{50} = 0.05 nM) exhibited excellent potency, selectivity, pharmacokinetic properties and >24 h efficacy in the SHR model following a single dose [25]. In a further study aiming at overcoming the unacceptable toxicity of **53**, a potent, orally active and brain penetrant inhibitor 3-[4-(2-hydroxyethyl)piperazin-1-yl]-7-(6-methoxypyridin-3-yl)-1-(2-propoxyethyl) pyrido[3, 4-b]pyrazin-2(1H)-one (IC_{50} = 0.2 nM) was identified together with 11 other fresh compounds as PDE5 inhibitors [26]. Subsequently, endeavors to further examine the SAR of pyrazinone derivatives and develop alternate approaches to effectively balance the potency, selectivity and PK profiles pointed to the discovery of another 30 novel PDE5 inhibitors with excellent potency, selectivity and PK profiles [27].

Therefore, the pyrazinone derivatives represent a promising group of PDE5 inhibitors which merit computational investigation. As a matter of fact, although computer-assisted drug design tools have been in use for over ten years in the field of drug development and a plenty of satisfying accomplishments have been achieved [28–32], the in silico studies on pyrazinone-based PDE5 inhibitors were seldom reported, with an exception of a computational research carried out on 30 amino-substituted pyrido[3,2b]pyrazinones by Tanwar et al. in 2010 [33]. Thus, molecular modeling studies more in-depth-and-range are indispensible for further development of novel pyrazinone-based PDE5 inhibitors.

In the present study, a total of 122 pyrazinone-based PDE5 inhibitors were used as (also by far the largest) dataset to build 3D-QSAR models using comparative molecular field analysis (CoMFA) [34,35] and comparative molecular similarity indices analysis (CoMSIA) tools [36]. Additionally, a test set of compounds which were not used for the establishment of the model were used to check the model's predictive ability. Moreover, the docking analysis and molecular dynamics (MD) simulation were also performed to elucidate the probable binding modes of these inhibitors. Finally, we performed 3D-QSAR study on 65 molecules of our dataset in order to examine their selectivity against PDE11. The developed models will hopefully aid in understanding the structure–activity relationship of these compounds and provide instruction for the design of novel PDE5 inhibitors.

2. Materials and methods

2.1. Dataset and biological activity

The dataset employed for the 3D-QSAR analyses consists of 122 pyrazinone-based PDE5 inhibitors (Tables S1–S7) [23–27]. As dependent variables in the QSAR analyses, their in vivo IC_{50} values, in M, were converted to pIC_{50} ($-lgIC_{50}$) values ranging from 6.27 to 11. In approximately a ratio of 4:1, the whole data set was divided into training set (96 compounds) and test set (26 compounds) on the basis that compounds in the test set represent similar range of biological activities and structural diversity to that of the training one.

In the modeling process, the 3D structures of all compounds were subjected to full geometry optimization using the sketch molecule module of SYBYL 6.9 package [37]. Partial atomic charges were calculated by the Gasteiger–Hückel method [38], and energy minimizations were demonstrated by using the Tripos force field [39] and the Powell conjugate gradient algorithm with a convergence criterion of 0.05 kcal/(mol Å).

2.2. Conformational sampling and alignment

Molecular alignment of compounds is a significant step in the development of CoMFA and CoMSIA models [40]. Presently, two different alignment methods have been applied to derive the best possible 3D-QSAR model. One is the ligand-based alignment, where the most potent compound 115 was chosen as a template to fit the remaining training and test sets of molecules by using the substructure-alignment function available in SYBYL. The common substructure is marked in bold (Fig. 1A), and the ligand-based alignment model is shown in Fig. 1B.

The other method is the receptor-based alignment. In this approach, the optimal conformation of each molecule after the docking process was selected through leave-one-out (LOO) cross-validation [41]. Subsequently, the partial atomic charges of the molecules were calculated by the Gasteiger–Hückel method [38]. The receptor-based alignment is shown in Fig. 1C.

2.3. CoMFA and CoMSIA field calculation

The aligned molecules were placed in a 3D grid box of 2.0 Å such that the entire set was included in the simulation box.

In CoMFA, steric and electrostatic fields with a distance-dependent dielectric at each grid point were calculated using a sp^3 carbon atom probe with a 1.52 Å van der Waals radius and a +1.0 charge using default settings in SYBYL. The energy cut-off values of 30 kcal/mol were set for both the steric and electrostatic fields. The steric and electrostatic interactions with each atom in the molecule were computed using the CoMFA standard scaling, with the probe atom located at each lattice point [42].

CoMSIA descriptors were derived employing the same lattice boxes as those used in the CoMFA calculations. In CoMSIA, with five fields (steric, electrostatic, hydrophobic, hydrogen bond (HB) donor and HB acceptor), a probe atom of charge +1.0, radius 1.0 Å, and hydrophobicity +1.0 was used to perform the calculation. The mutual distance between the probe atom and each molecule atom was evaluated with a Gaussian function. CoMSIA similarity indices

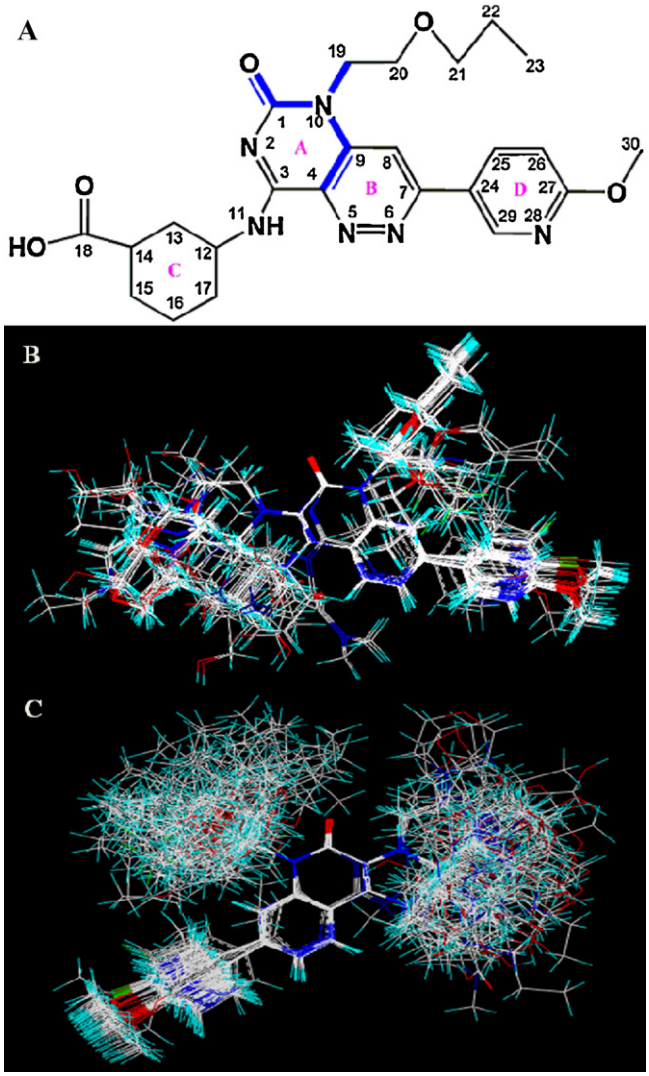

Fig. 1. (A) Compound 115 was used as a template for the ligand- and receptor-based alignments. The common substructure is shown in bold. Ligand- and receptor-based alignments of all the compounds are shown in panels (B) and (C), respectively. In panels (B) and (C), molecules are colored in white for common C, blue for N, red for O, green for F, and cyan for H atoms, respectively. (For interpretation of the references to color in the figure caption, the reader is referred to the web version of the article.)

(A_F) for molecule j with atom i at grid point q are calculated by Eq. (1):

$$A^q_{F,k}(j) = -\sum \omega_{\text{probe},k}\omega_{ik}e^{-\alpha r^2_{iq}} \quad (1)$$

where k represents the steric, electrostatic, hydrophobic, or H-bond donor or acceptor descriptor. $\omega_{\text{probe},k}$ is the probe atom with charge +1, radius 1.0 Å, hydrophobicity +1, H-bond donating +1 and H-bond accepting +1; ω_{ik} is the actual value of the physicochemical property k of atom i; attenuation factor $\alpha = 0.3$ (default value); r_{iq} is the mutual distance between the probe atom at grid point q and atom i of the test molecule.

2.4. 3D-QSAR model calculation and validation

For the sake of the generation of statistically reliable 3D-QSAR models, partial least squares (PLS) regression was adopted to analyze the data set by correlating the variation in their pIC_{50} values (the dependent variables) with variations in their CoMFA/CoMSIA interaction fields (the independent variables). PLS is effective in the prediction of a set of dependent variables from a large set of independent variables.

In PLS regression analyses, cross-validation analysis was done with the LOO method that one compound was removed from the dataset and its activity was predicted by employing the model derived from the rest of the dataset. Q^2, the cross-validated coefficient, was then obtained as a statistical index of the predictive power. Subsequently, a non-cross-validation analysis was applied, with the Pearson coefficient (R^2_{ncv}) and the standard error of estimates (SEE) calculated. At last, the CoMFA/CoMSIA results were graphically displayed by contour maps, in which the coefficients were generated with the "Stdev*Coeff" field type.

The predictive ability of the 3D-QSAR model was determined by using the compounds not included in the training set. A predictive R value was then obtained with the following formula:

$$R = \sqrt{\frac{\text{SD} - \text{PRESS}}{\text{SD}}} \quad (2)$$

where SD is the sum of the squared deviations between the biological activities of the test set and the mean activities of the training set molecules; PRESS designates the sum of squared deviation between the predicted and actual activities of the test set compounds.

2.5. Molecular docking

Molecular docking is a method usually adopted to calculate the protein–ligand interactions in that it is efficient to predict the potential ligand binding sites on the whole protein target [43]. In order to find the appropriate binding conformations and offer more insights into the interactions between PDE5 and its inhibitors, molecular docking analysis was performed by using the Surflex Dock implemented in SYBYL-X 1.1 [44]. The protein employed here is PDE5 (PDB code: 3HC8) [45] with a resolution of 1.9 Å and different conformers of all 122 ligands were docked into the binding site. During the docking process, the protomol-bloat which can be used to inflate the protomol and include nearby crevices was set to 0.5, and the protomol-threshold which is a factor determining how much the protomol can be buried in the protein was set to 1, respectively.

2.6. Molecular dynamics

Molecular dynamics simulations were conducted with GROMACS software package [46] using the GROMOS96 force field [47], with the docked structure as a start. The topology file for the ligand in protein was generated by the program PRODRG 2.5 [48,49]. With a cubic periodic box whose side length was 80.52 Å as the simulation cell, the minimum distance between box walls and the protein was set to be larger than 10 Å. The total charge was neutralized by placing 9 sodium ions randomly in the box. In the simulation system, the number of all the atoms was 55,550 including the protein complexes and waters, and the remaining box volume was filled by the simple point charge (SPC) water [50]. Prior to the simulation, the energy of the entire system was minimized using the steepest descent integrator for 14,631 steps, and then the system was equilibrated by a 100 ps MD simulation at 300 K. At last, a 5 ns simulation was performed with a time step of 2 fs. Specifically during the MD simulation process, the model used normal pressure and temperature (NPT) ensemble at 300 K with periodic boundary conditions; the temperature remained constant by the Berendsen thermostat; the value of the isothermal compressibility was set to 4.5×10^{-5} bar^{-1} while the pressure retained at 1 bar using the Parrinello–Rahman scheme [51]; electrostatic interactions were calculated with the particle mesh Ewald method [52]; cut-off distances for the calculation of Coulomb and van der Waals

Table 1
Summary of CoMFA and CoMSIA results.

PLS statistics	Ligand-based model		Receptor-based model	
	CoMFA	CoMSIA	CoMFA	CoMSIA
Q^2	0.584	0.561	0.466	0.516
R^2_{ncv}	0.884	0.833	0.919	0.987
SEE	0.323	0.386	0.267	0.108
F	112.575	73.918	204.486	668.103
R^2_{pre}	0.817	0.804	0.325	0.374
SEP	0.610	0.626	0.687	0.673
OPN	6	6	5	10
Contribution				
Steric	0.467	0.160	0.448	0.165
Electrostatic	0.533	0.427	0.552	0.425
Hydrophobic		0.413		0.411

Q^2, cross-validated correlation coefficient after the leave-one-out procedure; R^2_{ncv}, non-cross-validated correlation coefficient; SEE, standard error of estimate; F, ratio of R^2_{ncv} explained to unexplained $= R^2_{ncv}/(1 - R^2_{ncv})$; R^2_{pre}, predicted correlation coefficient for the test set of compounds; SEP, standard error of prediction; OPN, optimal number of principal components.

interactions were 1.0 and 1.4 nm, respectively; the MD simulations lasted for 5 ns in order to ensure the stability of the whole system.

3. Results and discussion

3.1. CoMFA and CoMSIA statistical results

The CoMFA and CoMSIA analyses were performed for both the ligand- and receptor-based alignment models with the same training set. The results obtained from both models are summarized in Table 1, where all the statistical parameters necessary to evaluate the predictive ability of the 3D-QSAR model, like the cross-validated correlation coefficient Q^2, non-cross-validated correlation coefficient R^2_{ncv}, and standard error of estimate SEE, F-statistic values as well as the optimum number of components OPN are analyzed.

The CoMFA model was obtained employing both the steric and electrostatic field descriptors. For the ligand-based modeling, a LOO cross-validated Q^2 of 0.584 with 6 optimum components and a high correlation coefficient (R^2_{ncv}) of 0.884 for the non-cross-validated final model as well as the SEE value (0.323) and an F-test value (112.575) show its good internal predictive capacity. As for the receptor-based modeling, the optimal results ($Q^2 = 0.466$ with 5 optimum components, $R^2_{ncv} = 0.919$) also demonstrate an appropriate internal predictability.

For the CoMSIA models, all five field descriptors (steric, electrostatic, hydrophobic, HB-donor and HB-acceptor) need to be considered since they are not always completely independent of each other and such dependency among individual fields may reduce the model significance and generalization [53,54]. Thus, a total of 31 kinds of possible descriptors' combinations were calculated with their respective Q^2 value and the optimum number of components, for estimating the most predictive CoMSIA model. For the ligand-based modeling, the model using the descriptors of steric, electrostatic and hydrophobic fields appears to be superior to the other models derived, of which only the best CoMSIA result is listed in Table 1. The ligand-based CoMSIA model has a Q^2 value of 0.561 with 6 optimum components, a high R^2_{ncv} value of 0.833, indicating its good predictive ability. Similarly, the receptor-based CoMSIA model, using the combination of steric, electrostatic and hydrophobic field descriptors also displays wonderful internal predictive ability.

In general, a cross-validated $Q^2 > 0.5$ is deemed as the proof of a satisfactory predictive 3D-QSAR model [55]. Nevertheless, it has been found that some models based on the training set possess high Q^2 values, while showing unfavorable predictive power in an external test set [56,57]. Hence, the LOO cross-validated Q^2 is insufficient to assess the predictive power of the QSAR models [58]. Therefore, an external test set of 26 compounds was used to validate the accuracy of both the ligand- and receptor-based models, respectively. The receptor-based models both got poor predictive coefficient R^2_{pre} of 0.325 for the CoMFA model and 0.374 for the CoMSIA model. Since the receptor-based model shows poor predictive power, we mainly discuss the ligand-based models in the following content.

Table 2
Comparison of CoMSIA results.

	SD	ED	SHE	SEHA
Q^2	0.372	0.531	0.561	0.569
R^2_{ncv}	0.86	0.913	0.833	0.814
R^2_{pre}	0.67	0.644	0.804	0.802

Q^2, cross-validated correlation coefficient after the leave-one-out procedure; R^2_{ncv}, non-cross-validated correlation coefficient; R^2_{pre}, predicted correlation coefficient for the test set of compounds (S, steric; E, electrostatic; H, hydrophobic; D/A, H-bond donor/acceptor).

Fig. 2 illustrates the correlation plots of the experimental versus the predicted pIC_{50} values of the training (filled blue diamond) and test sets (filled black square) for the optimal ligand-based CoMFA and CoMSIA models. For the CoMFA model, a predictive coefficient R^2_{pre} of 0.817 shows the high predictive ability of the model. Moreover, from Fig. 2A, we observe that the predicted values are very close to the experimental activities for the whole dataset with all the points evenly distributed around the regression line, indicating no systematic errors in the method. This good correlation between the predicted and experimental activity data proves the excellent predictivity of the CoMFA model. The CoMSIA model with the R^2_{pre} value of 0.804 also demonstrates the high predictive power for the potency of PDE5 inhibitors.

In addition, in order to explicate the crux of the modeling process, four CoMSIA results (shown in Table 2) were selected from altogether 31 field descriptor combinations that we have analyzed, for a comparative analysis. Considering (1) $Q^2 > 0.5$, (2) R^2_{ncv} and R^2_{pre} are the highest in value, (3) the difference between R^2_{ncv} and R^2_{pre} is smaller than 0.1, we select the model using the descriptors of steric, electrostatic and hydrophobic fields as our final result.

3.2. 3D-QSAR contour maps

After consideration of both the internal and external predictive powers of all the derived models, the StDev*Coeff contour maps of the best CoMFA and CoMSIA models were constructed to show the field effects on the target features. To aid in visualization, the most active inhibitor in the series (compound 115) is shown with the CoMFA and CoMSIA contour maps in Figs. 3 and 4, respectively.

For CoMFA steric fields, Fig. 3A shows the sterically favored (green) and disfavored (yellow) regions of the molecule. Around the 27-position, a large green contour is found, meaning that a bulky group is preferred here. For instance, compound 20 with —OCH_3 substitution is more active than compound 23 with —OH substituted at the 27-position. A green contour outside ring C indicates the favor for sterically bulky group in this region, which is consistent with the fact that a plenty of the most active compounds (compounds 115–122) have ring structures at the 12-position, and that compound 7 with a cyclic structure at ring C position is more potent than compound 6 without the substitution. In addition, a medium-size green region appears near the 21-position of the molecule, suggesting that a substituent of bulky steric at this position favors the biological activity. For example, compound 110 ($pIC_{50} = 9.36$) with —OPr substituent shows higher activity than compound 112 ($pIC_{50} = 8.83$) with —OEt at the 20-position.

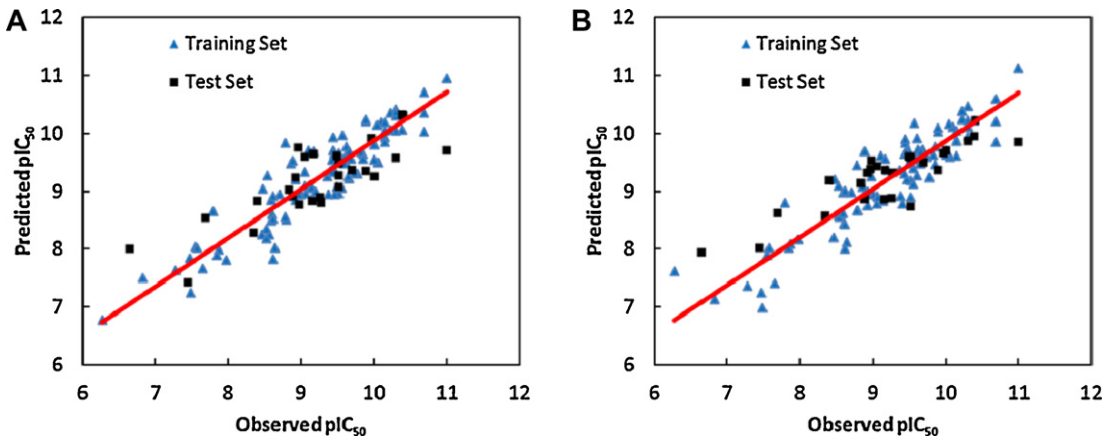

Fig. 2. The ligand-based correlation plots of the predicted versus the actual pIC_{50} values using the training (filled blue triangle) and the test (filled black square) set compounds based on (A) CoMFA and (B) CoMSIA models, respectively. (For interpretation of the references to color in the figure caption, the reader is referred to the web version of the article.)

Simultaneously, a yellow contour is displayed near the 25- and 26-position, suggesting bulky groups are disfavored here. Since none of the 122 molecules in regard have bulky substitution at these two positions, this contour result is reasonable.

For CoMFA electrostatic fields, Fig. 3B shows the electronegative favored (red) and electropositive favored (blue) regions of the molecule. A large blue contour around 12-position indicates that an electropositive group is favored at this position for improving the inhibitory activity. As an example, compound 43 (pIC_{50} = 9.77) with the electropositive substitution $-CH_2OCH_2CH_3$ displays higher potency than compound 47 (pIC_{50} = 8.53) with the electronegative substitution —COOH near the 12-position. At the same time, a big blue contour is found near 19- and 20-position showing preference toward more electropositive groups here, which can be illustrated by the fact that compounds 17–23 with a cyclohexane at 20-position are more active than compounds 24–30 with a $-CH_2OPr$ (less electropositive than cyclohexane) group at the same position, respectively. A medium sized red contour that indicates preference for electronegative substitution is observed around the 6-position of ring B, which can be explained by the comparison between compound 31 (pIC_{50} = 9.05) with positively charged atom C at 6-position and compound 34 (pIC_{50} = 10.15) with negatively charged atom N at the same position. Also, the fact that many of the most active compounds (compounds 113–122) all have negatively charged N substitution at 6-position is consistent with this finding. Additionally, both a red contour and a blue contour are found near 27-position, indicating the sensitivity of the inhibitory activity to the electrostatic feature of substituents at this position.

In our study, the CoMSIA model not only calculates the steric and electrostatic fields, but also uses the hydrophobic field to correlate with the inhibitory activity. As is illustrated in Fig. 4A, all green regions are located around the same positions as shown in the previous CoMFA steric contour map (Fig. 3A), further implying the correctness of the CoMFA model. Additionally in the CoMSIA electrostatic map, the red contour at 6-position, the blue contours around 12-, 19- and 20-positions, as well as both red and blue contours at 27-position align with the CoMFA electrostatic result. In a word, the CoMSIA steric and electrostatic contour maps are consistent with those obtained from the CoMFA model. Thus, we mainly discuss the hydrophobic contour map below.

Fig. 4C depicts the hydrophobic contour map of the CoMSIA model. A large yellow contour is found near ring C which implies that substitution by hydrophobic groups at this location is extended to result in a higher inhibitory activity, which can be validated by the high activities of compounds with cyclohexane-structures at ring C position such as compounds 95, 96, 107, 108 and 115. Also, the fact that compound 7 with hydrophobic substituent N-methyl(tetrahydro-2H-pyran-4-yl)methanamine at 2-position exhibits higher potency than compound 6 with hydrophilic group $-NH_2$ at the same position helps explain this result. A large white contour appears at the 5- and 6-position indicating that hydrophilic groups here are correlated with high activities of the molecules as exemplified by such active molecules as compounds 115–122 in the dataset with —N=N— at the 5- and 6-position, as well as by the lower activity of compound 31 (pIC_{50} = 9.05) with hydrophobic group —C=C— compared with compound 34 (pIC_{50} = 10.15) with

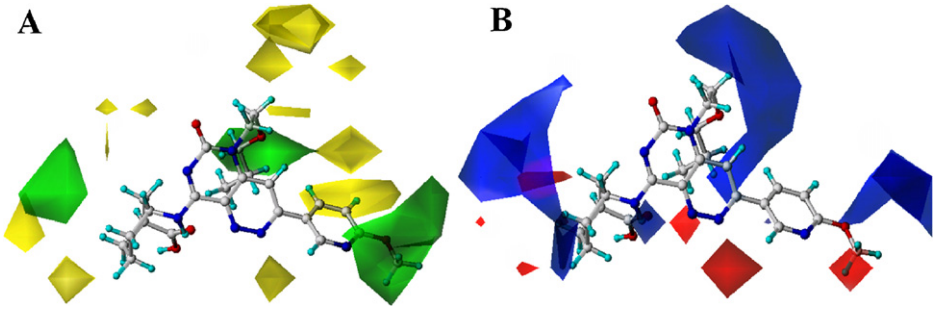

Fig. 3. CoMFA StDev*Coeff contour plots. (A) Steric (green/yellow) contour map in combination with compound 115. Green contours indicate regions where bulky groups increase activity; yellow contours indicate regions where bulky groups decrease activity. (B) Electrostatic contour map (red/blue) in combination with compound 115. Red contours indicate regions where negative charged groups increase activity; blue contours indicate regions where positive charged groups increase activity. The two maps generated depict regions having scaled coefficients 80% (favored) and 20% (disfavored). (For interpretation of the references to color in the figure caption, the reader is referred to the web version of the article.)

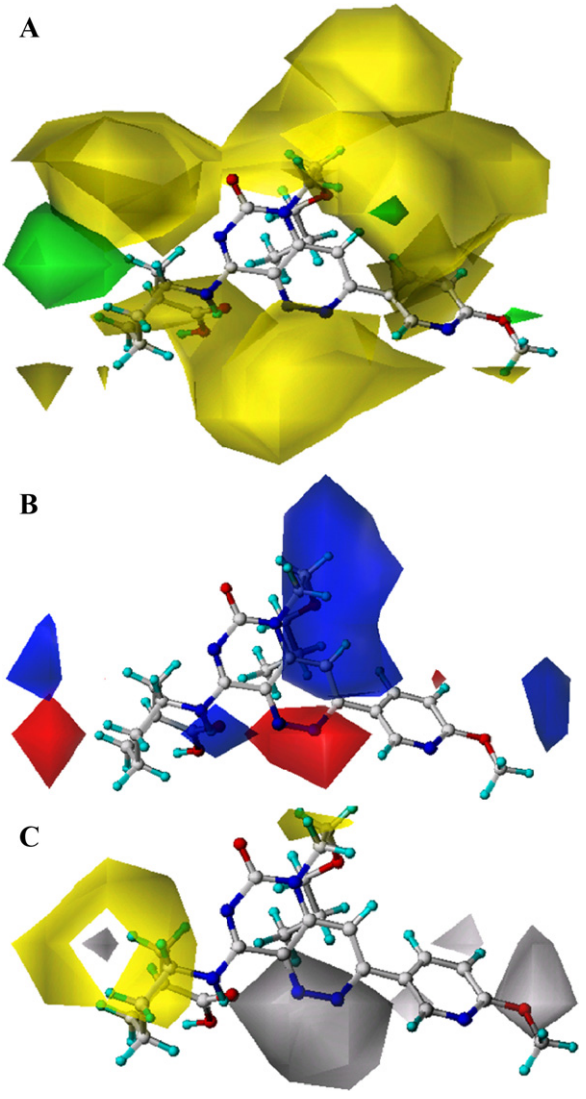

Fig. 4. CoMSIA StDev*Coeff contour plots. (A) Steric (green/yellow) contour map in combination with compound 115. Green contours (bulky groups favorable) and yellow contours (bulky groups unfavorable) represent 80% and 20% level contributions, respectively. (B) Electrostatic contour map (blue/red) in combination with compound 115. Blue contours (positively charged groups favorable) and red contours (negatively charged groups favorable) represent 70% and 30% level contributions, respectively. (C) Hydrophobic contour map (yellow/white) in combination with compound 115. Yellow contours (hydrophobic substituents favorable) and white contours (hydrophilic substituents favorable) represent 80% and 20% level contributions, respectively.

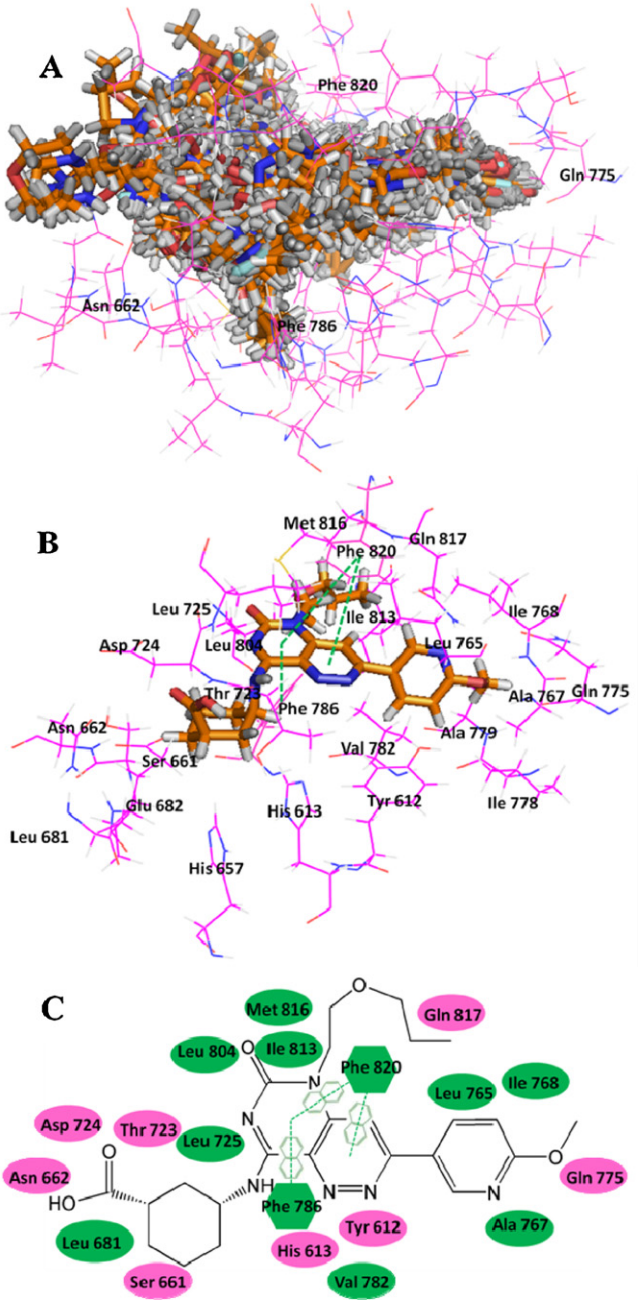

Fig. 5. (A) Docked conformations of all the 122 compounds into PDE5 (3HC8). (B) Docked conformation of compound 115 into 3HC8 with the π–π stacking interactions represented by green dashed lines. (C) 2D representation of compound 115 and the binding domain of PDE5. The green oval plates are for hydrophobic residues and the pink oval plates are for hydrophilic residues. The π–π stacking interactions are represented by a naphthyl icon and the corresponding amino acids Phe786 and Phe820 are represented by hexagons. (For interpretation of the references to color in the figure caption, the reader is referred to the web version of the article.)

hydrophilic group —N=C— at 5- and 6-position. A yellow contour is located near the 19-position, suggesting the favor for hydrophobic groups here. For instance, compounds 17, 28 and 29 are respectively more active than compounds 24, 25 and 26 due to the larger hydrophobicity of the —cyclohexane (ClogP = 3.35) than —CH_2OPr substituent (ClogP = 1.01). Additionally, a medium-size white contour near the 27-position indicates that hydrophilic groups are favored here. For example, compound 7 (pIC_{50} = 8.52) with —F substituted at 27-position exhibits lower potency than compound 20 (pIC_{50} = 9.52) with —OMe, which is more favorable at the same position.

3.3. Docking results

In order to explore the optimal orientation of the ligand in the binding pocket of the protein, docking studies were also carried out on the dataset [59]. In this study, all 122 compounds were docked into the possible active site of PDE5. The binding mode of the most potent compound 115 docked into the receptor (Fig. 5) is taken as an example for analysis. As seen from the figure, the active binding site generated consists of altogether 23 key amino acids including Leu725, Leu804, Leu765, Leu681, Phe820, Phe786, Ala767, Ala779, Ile768, Ile813, Ile778, Met816, Val782, Gln817, Gln775, Tyr612, Asp724, Thr723, Glu682, His613, His657, Ser661 and Asn662. From a 3D perspective, the binding pocket is observed to be in the shape of a bag that is one-sided open.

In Fig. 5B, hydrophobic amino acid residues Leu725 and Phe786 are found around the 12-position of ring C; hydrophobic amino acid residues Met816, Phe820, Leu804, and Ile813 are located near the 19-position, indicating that molecules with hydrophobic groups in these areas may possess high binding affinities to PDE5. Hydrophilic amino acid residues Tyr612 and His613 around the 5- and 6-positions suggest the disfavor of compounds with hydrophobic groups in these positions. These conclusions are in well agreement with our previous CoMSIA hydrophobic contour map.

It can be easily found that the aromatic residue in Phe820 forms face-to-face π–π stacking interaction with rings A and C, while Phe786 interacts with ring A by edge-to-face π–π stacking. Wang and Hobza have calculated the π–π interaction energies for a series of benzene and nitrogen that contain heterocyclic dimers and discovered that the interaction energy of the complex rises with the increase of nitrogen content of the heterocycles. These interactions each can contribute as much as 4 kcal/mol [60]. According to this theory, the more N atoms ring B has, the higher π–π interaction energies should be, and thus more favored for the binding of inhibitors to PDE5. However, it was discovered that the placement of the core pyridyl nitrogen at 8-position might lead to an unfavorable, repulsive interaction with the side-chain carbonyl [24]. Simultaneously, our research shows the preference for hydrophilic substitutions at 5- and 6-positions, so —C=N— substitution is more favorable than —N=N— group. Based on these two theories, N atoms are unfavorable on ring B. To reconcile the above three seemingly contradictory views, we initiate a new integrative theory regarding ring B that the N atom at 20-position is detrimental to the inhibitor activity and that the effect of N atoms at 5- and 6-position on compound activity is co-determined by both the hydrophobic force and π–π stacking interaction. For example, compound 32 is less active than compound 31 due to the placement of N atom at 8-position; compound 104 is more potent than compound 97, but less potent than compound 98 due to the different outcomes of hydrophobic and π–π stacking competition. In conclusion, both the ring A and, especially, the ring B play important roles in this binding pocket due to their ability to form π–π stacking interactions with the residues.

Our model also shows comparatively large empty spaces around the cyclohexane ring C, 21- and 27-positions indicating that in these regions the steric interaction may be favorable. Meanwhile, several crucial amino acid residues are found at some specific positions of the molecule. For example, residues Gln817, Leu765 and Ile768 are found at the 25- and 26-positions, implying that bulky groups at these positions may impair the activity. These results are also consistent with the above CoMFA model (Fig. 3A).

At present, only one study was carried out on the binding mode of compound 28 to PDE5 by examining the X-ray structure of the binding result [24]. The binding pocket is the same as the one obtained from our study, and π–π stacking interaction is also found as the major contribution to binding energy. However, their finding that the carbonyl at 1-position is held in position via a HB network is inconsistent with our docking result that no HB is observed between PDE5 and its bound inhibitor. The reason for such disparity may be that the compound they used (compound 28 with IC_{50} value of 2.9 nM) for binding feature analysis is different from the template compound 115 (IC_{50} = 0.01 nM) in our study. Supposedly, HBs are key factors for the binding mode when inhibitory activity is low but possibly become minor aspect when the activity is comparatively higher.

3.4. Molecular dynamics results

At present, a 5 ns simulation of the docked structure of 3HC8 with ligand 115 was carried out in order to obtain a dynamical figure of the conformational variations that occur in aqueous solution, aiming to investigate the conformational alterations taking place in

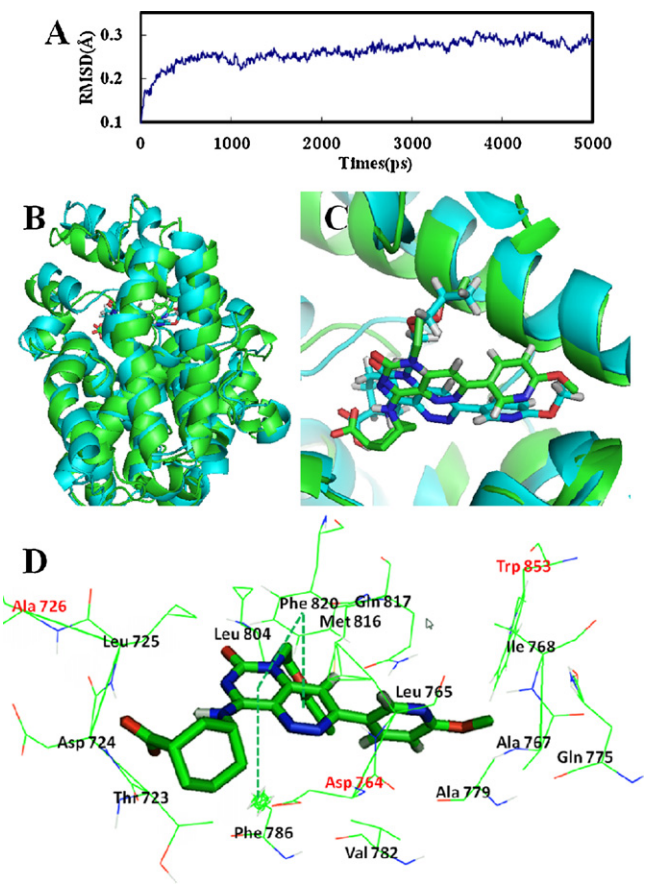

Fig. 6. (A) Plot of the root-mean-square deviation (RMSD) of docked complex versus the MD simulation time in the MD-simulated structures. (B and C) Projection of the superimposed backbone atoms of the average structure of the last 1 ns of the MD simulation (green) and the initial structure (cyan) for compound 115–3HC8 complex. (D) Conformation of compound 115 into 3HC8 after the MD simulation, with the π–π stacking interactions represented by green dashed lines and the amino acids that do not appear in the docking results colored in red. Compound 115 is represented as carbon-chain in cyan for the initial complex and carbon-chain in green for the lowest energy complex. (For interpretation of the references to color in the figure caption, the reader is referred to the web version of the article.)

ligand 115 and 3HC8. As a result, the RMSDs (all atoms) of the trajectory regarding their initial structure ranging from 0.1 to 0.3 Å are shown in Fig. 6A. After 2 ns, the RMSD of the complex reaches about 0.27 Å and remains constant around this value throughout the simulation, which clearly points to the metastability of the conformation after 2 ns of simulation for the docked complex structure. For clearance, a superposition of the average structure of the last 1 ns in the entire MD simulations and the initial docked structure is shown in Fig. 6B and C, where the cyan ribbon represents the initial structure for the docked complex, and the green ribbon denotes the average structure of the last 1 ns, with compound 115 represented as carbon-chain in cyan for the initial complex and carbon-chain in green for the average structure of the last 1 ns. Specifically, an average structure of the last 1 ns in the simulation was adopted because the use of an average structure from an MD simulation is generally more reliable compared to the use of a single crystal structure [61].

Fig. 6C demonstrates satisfactory overlap of the average structure extracted from MD simulations with the docked model of the complex. In addition, from Fig. 5D depicting the binding interactions including the prioritized π–π stacking interactions discussed in the docking result, we find no significant differences in terms of key amino acids and the binding mode, which further validates the rationality and validity of the docking model. One thing to notice, although the average of MD conformers in the last 1 ns may

conceal H-bond interactions that were probably achieved in particular sections of the simulation, such an H-bond was not observed either in the 3D-QSAR or docking results, suggesting that this interaction is not an essential characteristic for pyrazinone derivatives as PDE5 inhibitors [62].

4. Comparison with others

In this work, both the ligand- and receptor-based 3D-QSAR studies of 122 pyrazinone-based PDE5 inhibitors were carried out using CoMFA and CoMSIA tools. From the resultant models, the high Q^2, R^2_{ncv}, and R^2_{pre} values prove that the ligand-based CoMFA and CoMSIA models developed are statistically reliable and predictive. Furthermore, our 3D-QSAR models, docking and MD results are consistent well with each other. The resulting contour maps provide useful information about the intermolecular interactions of inhibitors with the surrounding environment.

As a matter of fact, 30 amino-substituted pyrido[3,2b]pyrazinones (compounds 1–30 in this article, with pIC_{50} (nM) values 6.27–9.52) as PDE5 inhibitors have been studied computationally by means of pharmacophore mapping using PHASE module of Schrödinger-9 by Tanwar et al. [33]. For the sake of clearance, the major structural features impacting the activity obtained from our present work and the features drawn by Tanwar et al. are shown in Fig. 7A and B respectively, where the similarities and differences can easily be observed.

By comparison, the interaction features obtained from our study and theirs are generally consistent with each other. Similarly, both studies imply the favor for electropositive and hydrophobic substituents on ring A, around 12- and 19-positions. However, it was found that inclusion of such electronegative groups as flouro, chloro and bromo at ring D would provide compounds with higher potency based on Tanwar's research, which is inconsistent with our findings that bulky hydrophilic groups are favorable around 27-position. One possible reason may be that the range of pIC_{50} (nM) values of 6.27–9.52 in their dataset of 30 amino-substituted pyrido[3,2b]pyrazinones is smaller compared with our values of 6.27–11. Furthermore, all our molecules with pIC_{50} (nM) values ranging from 9.52 to 11 share the same substitution (—OMe) at 27-position. This feature may be the cause of their high activity, and thus our conclusion that bulky hydrophilic groups are favored differs from theirs that electronegative groups at ring D increases inhibitory activity.

In order to gain more insights, we hereby further compare our results with those of other literatures studying various other types of PDE5 inhibitors. The X-ray structure of PDE5 co-crystallized with sildenafil, tadalafil and vardenafil unraveling the binding mode of the inhibitors was given by Eros et al. [63]. They located 9 key amino acids at the binding site, including Gln817, Phe820, His617, Asp764, His653, Asp654, His613, Tyr612 and Phe786. Amino acids Gln817, Phe820, His613, Tyr612 and Phe786 imply the overlap of their binding site and ours, while the other amino acids indicate the discrepancy.

Furthermore, Tomori et al. established a simple and rapid 2D/3D in silico selection method for PDE5 inhibitors from multimillion compounds' repositories and 14 PDE5 inhibitors with <1 μMIC_{50} values were identified [64]. The binding interactions are displayed between the protein and the best hit compound identified by this method in Fig. 7C. Notably, their key amino acids conform with ours around ring A, ring D and atoms 19–23, which helps to explain the commonality of potent PDE 5 inhibitors.

In addition, Yoo's 3D-QSAR study on sildenafil analogues as PDE5 inhibitors [65] suggests the favor for bulky and hydrophobic features on ring C (shown in Fig. 7D), which is similar with our results.

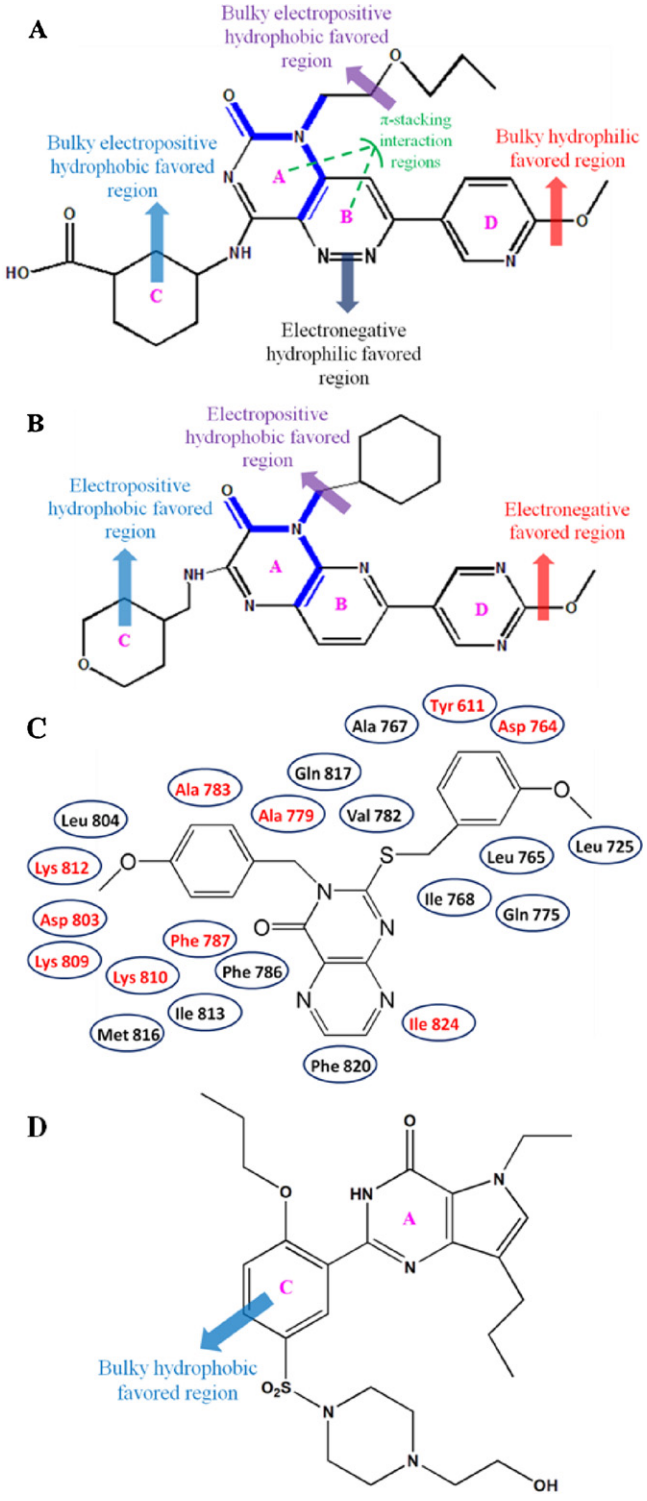

Fig. 7. (A) Key structural features of ligand 115 impacting the activity obtained from our present work. (B) Features of compound PDE030 obtained by Tanwar et al. [33]. (C) Protein interaction map of the best hit compound selected by 3D docking of the 2D similarity search results obtained by Tomori et al. [64]. (D) Features obtained by Yoo et al. [65]. The most active PDE5 inhibitors in each respective dataset are shown as templates in Fig. 7A–D respectively. In (A), green dash lines represent $\pi-\pi$ stacking interaction regions and other arrows represent the specific interaction regions. (For interpretation of the references to color in the figure caption, the reader is referred to the web version of the article.)

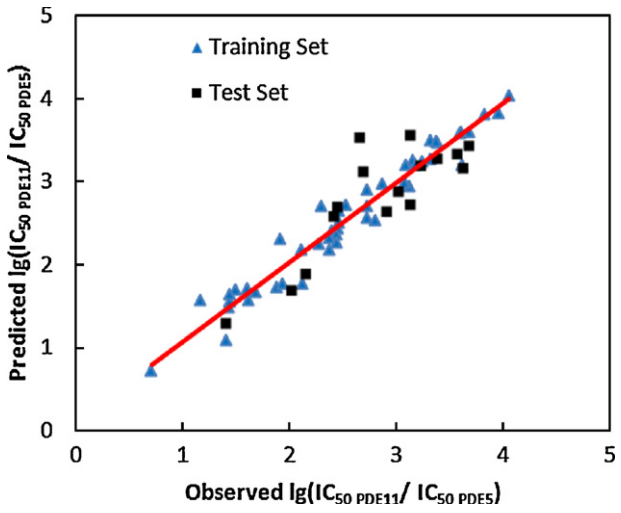

Fig. 8. The CoMFA correlation plot of the experimental versus the predicted $lg(IC_{50,PDE11}/IC_{50,PDE5})$ values of the training (filled blue triangle) and the test (filled black square) sets. (For interpretation of the references to color in the figure caption, the reader is referred to the web version of the article.)

The above comparisons between results of ours and others' indicate the similarities of various types of PDE5 inhibitors, regarding favorable substitutions and binding modes, which may be helpful for designing potential PDE5 inhibitors for desired activity.

Noticeably, subtype selectivity of PDEs were reported to be an important parameter in drug design approaches [66,67]. PDEs have altogether 11 subfamilies where PDE5 has only one subtype, PDE5A. Therefore, the selectivity of our molecules toward the PDE subfamilies is worthy of further research.

In the present study, only 65 molecules of our dataset were reported of their selectivity toward PDE11. Hence, we performed 3D-QSAR study on these 65 molecules in order to examine their selectivity toward PDE11. Specifically, the selectivity is represented by $lg(IC_{50,PDE11}/IC_{50,PDE5})$ values ranging from 0.71 to 4.06. In approximately a ratio of 3:1, the whole data set was divided into training set (49 compounds) and test set (16 compounds) on the basis that compounds in the test set represent similar range of biological activities and structural diversity to that of the training one. As a result, the CoMFA model described by steric field displays the optimum statistics that suggest the high predictive ability of the model: LOO cross-validated Q^2 of 0.500 with 8 optimum components, R^2_{ncv} of 0.954, R^2_{pre} of 0.720, SEE value of 0.192, and *F*-test value of 102.613. The corresponding correlation plot is illustrated in Fig. 8.

From the contour map of our best modeling result, where compound 108 with the highest $lg(IC_{50,PDE11}/IC_{50,PDE5})$ value was chosen as a template shown in Fig. 9, we observe a large green contour outside ring C indicating the favor for sterically bulky group in this region. In addition, the yellow region near the 21-position of the molecule suggests that a substituent of bulky steric at this position disfavors the selectivity of PDE5 against PDE11.

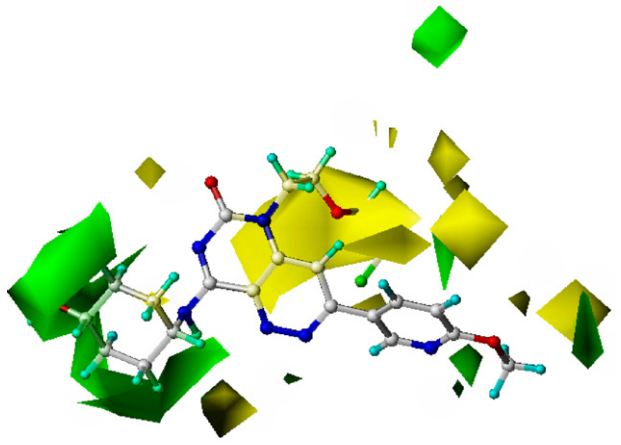

Fig. 9. CoMFA steric (green/yellow) contour map in combination with compound 108. Green contours indicate regions where bulky groups increase selectivity; yellow contours indicate regions where bulky groups decrease selectivity. The map generated depicts regions having scaled coefficients 80% (favored) and 20% (disfavored). (For interpretation of the references to color in the figure caption, the reader is referred to the web version of the article.)

5. Conclusion

Our main findings are: (1) Introduction of bulky, electropositive and hydrophobic substituents at 12- and 19-positions can increase the biological activities. (2) N atom at 8-position is detrimental to the inhibitor activity, and the effect of N atoms at 5- and 6-positions on compound activity is co-determined by both the hydrophobic force and the π–π stacking interaction. (3) Bulky and hydrophilic substitutions are favored at the 27-position of ring D. (4) Electronegative and hydrophilic substitutions around 5- and 6-positions increase the inhibitory activity. (5) Hydrophobic forces and π–π stacking interaction with Phe786 and Phe820 are crucial in determining the binding of pyrazinone derivatives to PDE5. (6) Bulky substitutions around ring C favors selectivity against PDE11, while bulky groups near the 21-position disfavor the selectivity.

In conclusion, all these results may be of help for better understanding of the structural requirements for improving the activity of inhibitors and the design of novel and potent PDE5 inhibitors.

Acknowledgments

Thanks for the financial support given by the National Natural Science Foundation of China (Grant Nos. 10801025 and 30973590), the National High Technology Research and Development Program ("863") of China (No. 2009AA02Z205). G.H. Li also appreciates the supports from the National Natural Science Foundation of China (31070641), the National Key Basic Research Development Program (2012CB721000) and "Hundreds Talents Program" of the Chinese Academy of Sciences.

Appendix A. Supplementary data

Supplementary data associated with this article can be found, in the online version, at http://dx.doi.org/10.1016/j.jmgm.2012.07.003.

References

[1] W.W. Dinsmore, Available and future treatments for erectile dysfunction, Clinical Cornerstone 1 (2005) 37–44.
[2] A.L. Burnett, Phosphodiesterase 5 mechanisms and therapeutic applications, American Journal of Cardiology 96 (2005) 29–31.
[3] S.K. Kulkarni, C.S. Patil, Phosphodiesterase 5 enzyme and its inhibitors: update on pharmacological and therapeutical aspects, Methods and Findings in Experimental and Clinical Pharmacology 26 (2004) 789.
[4] Y.H. Jeon, Y.S. Heo, C.M. Kim, Y.L. Hyun, T.G. Lee, S. Ro, J.M. Cho, Phosphodiesterase: overview of protein structures, potential therapeutic applications and recent progress in drug development, Cellular and Molecular Life Sciences 62 (2005) 1198–1220.
[5] P. Kanthapillai, T.J. Lasserson, E.H. Walters, Phosphodiesterase five inhibitors for pulmonary hypertension, Cochrane Database of Systematic Reviews 18 (2004) CD003562.
[6] J. Prickaerts, A. Sik, W.C.G. van Staveren, G. Koopmans, H.W.M. Steinbusch, F.J. van der Staay, J. de Vente, A. Blokland, Phosphodiesterase type 5 inhibition improves early memory consolidation of object information, Neurochemistry International 45 (2004) 915–928.

[7] S. Hood, M. Kirby, PDE-5 inhibitors—a summary, The British Journal of Diabetes & Vascular Disease 4 (2004) 383–386.
[8] I. Eardley, C. Donatucci, J. Corbin, A. El-Meliegy, K. Hatzimouratidis, K. McVary, R. Munarriz, S.W. Lee, Pharmacotherapy for erectile dysfunction, Journal of Sexual Medicine 7 (2010) 524–540.
[9] P. Dorsey, C. Keel, M. Klavens, W.J. Hellstrom, Phosphodiesterase type 5 (PDE5) inhibitors for the treatment of erectile dysfunction, Expert Opinion on Pharmacotherapy 11 (2010) 1109–1122.
[10] N.K. Terrett, A.S. Bell, D. Brown, P. Ellis, Sildenafil (VIAGRA), a potent and selective inhibitor of type 5 cGMP phosphodiesterase with utility for the treatment of male erectile dysfunction, Bioorganic & Medicinal Chemistry Letters 6 (1996) 1819–1824.
[11] I. Eardley, J. Cartledge, Tadalafil (Cialis) for men with erectile dysfunction, International Journal of Clinical Practice 56 (2002) 300–304.
[12] M. Gupta, A. Kovar, B. Meibohm, The clinical pharmacokinetics of phosphodiesterase-5 inhibitors for erectile dysfunction, Journal of Clinical Pharmacology 45 (2005) 987–1003.
[13] F. Sommer, Potency and selectivity of Vardenafil: a phospho-diesterase type 5 inhibitor, Expert Opinion on Drug Metabolism & Toxicology 1 (2005) 295–301.
[14] R.C. Kukreja, R. Ockaili, F. Salloum, C. Yin, J. Hawkins, A. Das, L. Xi, Cardioprotection with phosphodiesterase-5 inhibition—a novel preconditioning strategy, Journal of Molecular and Cellular Cardiology 36 (2004) 165–173.
[15] C.Y. Chen, Y.H. Chang, D.T. Bau, H.J. Huang, F.J. Tsai, C.H. Tsai, C.Y.C. Chian, Ligand-based dual target drug design for H1N1: swine flu—a preliminary first study, Journal of Biomolecular Structure and Dynamics 27 (2009) 171–178.
[16] G.B. Brock, C.G. McMahon, K.K. Chen, T. Costigan, W. Shen, V. Watkins, G. Anglin, S. Whitaker, Efficacy and safety of Tadalafil for the treatment of erectile dysfunction: results of integrated analyses, Journal of Urology 168 (2002) 1332–1336.
[17] H. Porst, R. Rosen, H.P. Nathan, I. Goldstein, F. Giuliano, E. Ulbrich, T. Bandel, Efficacy and safety of vardenafil, a new, oral, selective phosphodiesterase type 5 inhibitor, in patients with erectile dysfunction: the first at-home clinical trial, International Journal of Impotence Research 13 (2001) 192–199.
[18] G. Xia, J. Li, A. Peng, S. Lai, S. Zhang, J. Shen, Z. Liu, X. Chena, R. Ji, Synthesis and phosphodiesterase 5 inhibitory activity of novel pyrido[12-e]purin-4(3H)-one derivatives, Bioorganic and Medicinal Chemistry Letters 15 (2005) 2790–2794.
[19] M.J. Palmer, A.S. Bell, D.N. Fox, D.G. Brown, Design of second generation phosphodiesterase 5 inhibitors, Current Topics in Medicinal Chemistry 7 (2007) 405–419.
[20] S. Abel, K.C. Beaumont, C.L. Crespi, M.D. Eve, L. Fox, R. Hyland, B.C. Jones, G.J. Muirhead, D.A. Smith, R.F. Venn, D.K. Walker, Potential role for P-glycoprotein in the nonproportional pharmacokinetics of UK-343664 in man, Xenobiotica 31 (2001) 665–676.
[21] M.E. Bunnage, J.P. Mathias, S.D.A. Street, A. Wood, K.C. Beaumont, S.A. Ballard, Design of potent and selective PDE5 inhibitors for treatment of MED, in: ACS Meeting 224th, 2002.
[22] D.A. Pissarnitski, T. Asberom, C.D. Boyle, S. Chackalamannil, M. Chintala, J.W. Clader, W.J. Greenlee, Y. Hu, S. Kurowski, J. Myers, J. Palamanda, A.W. Stamford, S. Vemulapalli, Y. Wang, P. Wang, P. Wu, R. Xu, SAR development of polycyclic guanine derivatives targeted to the discovery of a selective PDE5 inhibitor for treatment of erectile dysfunction, Bioorganic and Medicinal Chemistry Letters 14 (2004) 1291–1294.
[23] D.R. Owen, J.K. Walker, E.J. Jacobsen, J.N. Freskos, R.O. Hughes, D.L. Brown, A.S. Bell, D.G. Brown, C. Phillips, B.V. Mischke, J.M. Molyneaux, Y.M. Fobian, S.E. Heasley, J.B. Moon, W.C. Stallings, D.J. Rogier, D.N. Fox, M.J. Palmer, T. Ringer, M.R. Lens, J.W. Cubbage, R.M. Blevis-Bal, A.G. Benson, B.A. Acker, T.M. Maddux, M.B. Tollefson, B.R. Bond, A. Macinnes, Y. Yu, Identification, synthesis and SAR of amino substituted pyrido[3,2b]pyrazinones as potent and selective PDE5 inhibitors, Bioorganic and Medicinal Chemistry Letters 19 (2009) 4088–4091.
[24] R.O. Hughes, J.K. Walker, J.W. Cubbage, Y.M. Fobian, D.J. Rogier, S.E. Heasley, R.M. Blevis-Bal, A.G. Benson, D.R. Owen, E.J. Jacobsen, J.N. Freskos, J.M. Molyneaux, D.L. Brown, W.C. Stallings, B.A. Acker, T.M. Maddux, M.B. Tollefson, J.M. Williams, J.B. Moon, B.V. Mischke, J.M. Rumsey, Y. Zheng, A. Macinnes, B.R. Bond, Y. Yu, Investigation of aminopyridiopyrazinones as PDE5 inhibitors: evaluation of modifications to the central ring system, Bioorganic and Medicinal Chemistry Letters 19 (2009) 4092–4096.
[25] R.O. Hughes, J.K. Walker, D.J. Rogier, S.E. Heasley, R.M. Blevis-Bal, A.G. Benson, E.J. Jacobsen, J.W. Cubbage, Y.M. Fobian, D.R. Owen, J.N. Freskos, J.M. Molyneaux, D.L. Brown, B.A. Acker, T.M. Maddux, M.B. Tollefson, J.B. Moon, B.V. Mischke, J.M. Rumsey, Y. Zheng, A. MacInnes, B.R. Bond, Y. Yu, Optimization of the aminopyridopyrazinones class of PDE5 inhibitors: discovery of 3-[(trans-4-hydroxycyclohexyl)amino]-7-(6-methoxypyridin-3-yl)-1-(2-propoxyethyl)pyrido[3,4-b]pyrazin-2(1H)-one, Bioorganic and Medicinal Chemistry Letters 19 (2009) 5209–5213.
[26] R.O. Hughes, D.J. Rogier, E.J. Jacobsen, J.K. Walker, A. Macinnes, B.R. Bond, L.L. Zhang, Y. Yu, Y. Zheng, J.M. Rumsey, J.L. Walgren, S.W. Curtiss, Y.M. Fobian, S.E. Heasley, J.W. Cubbage, J.B. Moon, D.L. Brown, B.A. Acker, T.M. Maddux, M.B. Tollefson, B.V. Mischke, D.R. Owen, J.N. Freskos, J.M. Molyneaux, A.G. Benson, R.M. Blevis-Bal, Design, synthesis, and biological evaluation of 3-[4-(2-hydroxyethyl)piperazin-1-yl]-7-(6-methoxypyridin-3-yl)-1-(2-propoxyethyl)pyrido[3,4-b]pyrazin-2(1H)-one, a potent, orally active, brain penetrant inhibitor of phosphodiesterase 5 (PDE5), Journal of Medicinal Chemistry *53* (2010) 2656–2660.
[27] R.O. Hughes, T. Maddux, D.J. Rogier, S. Lu, J.K. Walker, E.J. Jacobsen, J.M. Rumsey, Y. Zheng, A. Macinnes, B.R. Bond, S. Han, Investigation of the pyrazinones as PDE5 inhibitors: evaluation of regioisomeric projections into the solvent region, Bioorganic and Medicinal Chemistry Letters 21 (2011) 6348–6352.
[28] J. Liu, F. Wang, Z. Ma, X. Wang, Y. Wang, Structural determination of three different series of compounds as Hsp90 inhibitors using 3D-QSAR modeling, molecular docking and molecular dynamics methods, International Journal of Molecular Science 12 (2011) 946–970.
[29] J. Liu, H. Zhang, Z. Xiao, F. Wang, X. Wang, Y. Wang, Combined 3D-QSAR, molecular docking and molecular dynamics study on derivatives of peptide epoxyketone and tyropeptin-boronic acid as inhibitors against the β5 subunit of human 20S proteasome, International Journal of Molecular Science 12 (2011) 1807–1835.
[30] S. Wei, Z. Ji, H. Zhang, J. Zhang, Y. Wang, W. Wu, Isolation, biological evaluation and 3D-QSAR studies of insecticidal/narcotic sesquiterpene polyol esters, Journal of Molecular Modeling 17 (2011) 681–693.
[31] X. Wang, X. Xu, M. Ma, W. Zhou, Y. Wang, L. Yang, pH-dependent channel gating in connexin26 hemichannels involves conformational changes in N-terminus, Biochimica Et Biophysica Acta, http://dx.doi.org/10.1016/j.bbamem.2011.12.027, in press.
[32] X. Xu, R. Li, M. Ma, X. Wang, Y. Wang, H. Zou, Multidrug resistance protein P-glycoprotein does not recognize nanoparticle C60: experiment and modeling, Soft Matter 8 (2012) 2915–2923.
[33] O. Tanwar, R. Saha, M.M. Alam, M. Akhtar, 3D-QSAR of amino-substituted pyrido[3,2B]pyrazinones as PDE-5 inhibitors, Medicinal Chemistry Research 21 (2012) 202–211.
[34] R.D. Cramer, J.D. Bunce, D.E. Patterson, I.E. Frank, Crossvalidation, bootstrapping, and partial least squares compared with multiple regression in conventional QSAR studies, Quantitative Structure–Activity Relationships 7 (1988) 18–25.
[35] R.D. Cramer, D.E. Patterson, J.D. Bunce, Comparative molecular-field analysis (CoMFA). 1. Effect of shape on binding of steroids to carrier proteins, Journal of the American Chemical Society 110 (1988) 5959–5967.
[36] G. Klebe, U. Abraham, T. Mietzner, Molecular similarity indices in a comparative analysis (CoMSIA) of drug molecules to correlate and predict their biological activity, Journal of Medicinal Chemistry 37 (1994) 4130–4146.
[37] SYBYL, Version 6.9, Tripos Inc., St. Louis, MO, USA, 1699.
[38] J. Gasteiger, M. Marsili, Iterative partial equalization of orbital electronegativity—a rapid access to atomic charges, Tetrahedron 36 (1980) 3219–3228.
[39] M. Clark, R.D. Cramer, N. Van Opdenbosch, Validation of the general purpose tripos 5.2 force field, Journal of Computational Chemistry 10 (1989) 982–1012.
[40] M.D.M. Abdul Hameed, A. Hamza, J. Liu, C.G. Zhan, Combined 3D-QSAR modeling and molecular docking study on indolinone derivatives as inhibitors of 3-phosphoinositide-dependent protein kinase-1, Journal of Chemical Information and Modeling 48 (2008) 1760–1772.
[41] C.R. Rao, Y. Wu, Linear model selection by cross-validation, Journal of Statistical Planning and Inference 128 (2005) 231–240.
[42] H. Kubinyi, QSAR and 3D QSAR in drug design. Part 1: methodology, Drug Discovery Today 2 (1997) 457–467.
[43] M. Shahlaei, A.M. Sobhani, K. Mahnam, A. Fassihi, L. Saghaie, M. Mansourian, Homology modeling of human CCR5 and analysis of its binding properties through molecular docking and molecular dynamics simulation, Biochimica Et Biophysica Acta 1808 (2011) 802–817.
[44] SYBYL-X, Version 1.1, Tripos Inc., St. Louis, MO, USA, 2009.
[45] <http://www.rcsb.org/pdb>.
[46] H.J.C. Berendsen, D. van der Spoel, R. van Drunen, GROMACS: a message-passing parallel molecular dynamics implementation, Computer Physics Communications 91 (1995) 43–56.
[47] E. Lindahl, B. Hess, D. Van der Spoel, GROMACS 3.0: a package for molecular simulation and trajectory analysis, Journal of Molecular Modeling 7 (2001) 306–317.
[48] D.M.F. Aalten, R. Bywater, J.B.C. Findlay, M. Hendlich, R.W.W. Hooft, G. Vriend, PRODRG, a program for generating molecular topologies and unique molecular descriptors from coordinates of small molecules, Journal of Computer-Aided Molecular Design 10 (1996) 255–262.
[49] A.W. Schuttelkopf, D.M.F. van Aalten, PRODRG: a tool for high-throughput crystallography of protein–ligand complexes, Acta Crystallographica Section D: Biological Crystallography 60 (2004) 1355–1363.
[50] H.J.C. Berendsen, J.P.M. Postma, W.F. Van Gunsteren, J. Hermans, Interaction models for water in relation to protein hydration, in: B. Pullman (Ed.), Intermolecular Forces, Reidel, Dordrecht, 1981, pp. 331–342.
[51] M. Parrinello, A. Rahman, Polymorphic transitions in single crystals: a new molecular dynamics method, Journal of Applied Physics 52 (1981) 7182–7190.
[52] J.H. Lin, A.L. Perryman, J.R. Schames, J.A. McCammon, Computational drug design accommodating receptor flexibility: the relaxed complex scheme, Journal of the American Ceramic Society 124 (2002) 5632–5633.
[53] M. Bohm, J. Sturzebecher, G. Klebe, Three-dimensional quantitative structure–activity relationship analyses using comparative molecular field analysis and comparative molecular similarity indices analysis to elucidate selectivity differences of inhibitors binding to trypsin, thrombin, and factor Xa, Journal of Medicinal Chemistry 42 (1999) 458–477.
[54] G. Bringmann, C. Rummey, 3D QSAR investigations on antimalarial naphthylisoquinoline alkaloids by comparative molecular similarity indices analysis (CoMSIA), based on different alignment approaches, Journal of Chemical Information and Computer Sciences 43 (2003) 304–316.
[55] G.M. Sperandio da Silva, C.M.R. SantAnna, E.J. Barreiro, A novel 3D-QSAR comparative molecular field analysis (CoMFA) model of imidazole and

quinazolinone functionalized p38 MAP kinase inhibitors, Bioorganic and Medicinal Chemistry 12 (2004) 3159–3166.
[56] G. Wang, Y. Li, X. Liu, Y. Wang, Understanding the aquatic toxicity of pesticide: structure–activity relationship and molecular descriptors to distinguish the ratings of toxicity, QSAR Combinatorial Science 28 (2009) 1418–1431.
[57] Q. Wang, R.H. Mach, D.E. Reichert, Docking and 3D-QSAR studies on isatin sulfonamide analogues as caspase-3 inhibitors, Journal of Chemical Information and Modeling 49 (2009) 1963–1973.
[58] A. Golbraikh, A. Tropsha, Beware of q^2!, Journal of Molecular Graphics & Modelling 20 (2002) 269–276.
[59] D.B. Kitchen, H. Decornez, J.R. Furr, J. Bajorath, Docking and scoring in virtual screening for drug discovery: methods and applications, Nature Reviews. Drug Discovery 3 (2004) 935–949.
[60] W. Wang, P. Hobza, Theoretical study on the complexes of benzene with isoelectronic nitrogen-containing heterocycles, ChemPhysChem 9 (2008) 1003–1009.
[61] H.W.T. van Vlijmen, M. Schaefer, M. Karplus, Improving the accuracy of protein pK_a calculations: conformational averaging versus the average structure, Proteins 33 (1998) 145–158.
[62] E.D. Scheeff, J.M. Briggs, S.B. Howell, Molecular modeling of the intrastrand guanine–guanine DNA adducts produced by cisplatin and oxaliplatin, Molecular Pharmaceutics 56 (1999) 633–643.
[63] D. Eros, C.S. Kis, R. Kiss, G. Keri, B.H. Barakonyi, I. Kovesdi, L. Orfi, Structure–activity relationships of PDE5 inhibitors, Current Medicinal Chemistry 15 (2008) 1570–1585.
[64] T. Tomori, I. Hajdu, L. Barna, Z. Lorincz, S. Cseh, G. Dorman, Combining 2D and 3D in silico methods for rapid selection of potential PDE5 inhibitors from multimillion compounds' repositories: biological evaluation, Molecular Diversity 16 (2012) 59–72.
[65] J. Yoo, K.M. Thai, D.K. Kim, J.Y. Lee, H.J. Park, 3D-QSAR studies on sildenafil analogues, selective phosphodiesterase 5 inhibitors, Bioorganic & Medicinal Chemistry Letters 17 (2007) 4271–4274.
[66] P. Srivani, E. Srinivas, R. Raghu, G.N. Sastry, Molecular modeling studies of pyridopurinone derivatives—potential phosphodiesterase 5 inhibitors, Journal of Molecular Graphics and Modelling 26 (2007) 378–390.
[67] P. Srivani, D. Usharani, E.D. Jemmis, G.N. Sastry, Subtype selectivity in phosphodiesterase 4 (PDE4): a bottleneck in rational drug design, Current Pharmaceutical Design 14 (2008) 3854–3872.